

Submitted to the Editor of the Astrophysical Journal

Shadowing of the Nascent Jet in NGC 4261 by a Line-Emitting Supersonic Accretion Disk

Siming Liu

Department of Physics, The University of Arizona, Tucson, AZ 85721

Michael J. Fromerth¹

Department of Physics, The University of Arizona, Tucson, AZ 85721

and

Fulvio Melia²

Department of Physics and Steward Observatory, The University of Arizona, Tucson, AZ
85721

ABSTRACT

NGC 4261 (3C 270) is a low-luminosity radio galaxy with two symmetric kiloparsec-scale jets. Earlier *Hubble Space Telescope* observations indicated the presence of a hundred-parsec scale disk of cool dust and gas surrounding a central, supermassive ($\sim 4.9 \times 10^8 M_\odot$) black hole. The recent detection of free-free radio absorption by a small, geometrically-thin disk, combined with earlier studies of the disk's large scale properties, provide the strictest constraints to date on the nature of the accretion process in this system. We show here that a supersonic disk, illuminated by the active galactic nucleus (AGN), can not only account for the observed radio shadowing, but can also produce the optical broad lines emitted from this region. At large radii, the gas is optically-thin because the ram pressure due to turbulence is much larger than the thermal pressure of the gas. At smaller radii, but beyond a critical radius r_c , line cooling dominates over gravitational dissipation and the gas is effectively cooled down to temperatures below 10^4 K. Within r_c , however, heating due to

¹NSF Graduate Fellow.

²Sir Thomas Lyle Fellow and Miegunyah Fellow.

the release of gravitational energy overwhelms line cooling and the gas falls onto the unstable portion of the cooling curve. Because cooling is quite inefficient under these conditions, the plasma is heated very quickly to a temperature close to its virial value as it falls toward the central engine. Thermal pressure of the gas dominates the turbulent ram pressure at a radius $\sim (2/3) r_c$, below which the flow probably becomes advection dominated. The disk is optically-thin to UV and X-ray radiation within r_c , so the ionizing radiation from the AGN is preferentially absorbed near r_c , affecting the disk structure significantly. To include the ensuing photoionization effect, we have used the algorithm Cloudy with additional heating introduced by gravitational dissipation to calculate the temperature profile and line emission from the disk in a self-consistent manner. The results of our model calculation are consistent with current multiwavelength observations of the disk in this source.

Subject headings: accretion—black hole physics—Galaxy: NGC 4261—hydrodynamics—turbulence—line: formation

1. Introduction

The development of supermassive black hole accretion theories has always been limited by observations (Pringle 1981). This has been changing quickly during the past few years, with increasingly higher resolution observations being made over a wide frequency range. For example, the *Chandra X-ray Observatory* (*Chandra*) and the *Hubble Space Telescope* (*HST*) both have sub-arcsec scale resolutions, while the *Very Large Baseline Interferometer* (*VLBI*) can resolve structures on sub-milliarcsec scale. By combining multiwavelength observations from these different instruments, we can obtain very strict constraints on the nature of accretion around supermassive black holes.

While the innermost structures of AGNs remain unresolved (however, cf. Melia & Falcke 2001 regarding the Galactic center), the current data are good enough to constrain the properties of the large-scale accretion disks that are presumably feeding the central engines. A better understanding of these large-scale disks is not only tenable, but will also provide significant implications on the nature of the AGNs. Most of the relevant theoretical work to date is based on the standard α -disk prescription (Shakura & Sunyaev 1973), in which the accretion disk at large radii is supported by the thermal pressure of the gas (see, e.g., Hubeny 1990; Huré et al. 1994; Collin & Huré 1999). This may not be the entire story, however, as some observations suggest that turbulence is prominent in the disks of many

radio galaxies (Ferrarese, Ford & Jaffe 1996; Ferrarese & Ford 1999; van Langevelde et al. 2000). In addition, the inner disk is irradiated (Maloney, Hollenbach & Tielens 1996), which should affect, e.g., its physical properties and line emission characteristics.

At a distance of only 30 Mpc, the FR I radio galaxy NGC 4261 provides us an exceptional opportunity to investigate these new effects. Harboring a $4.9 \times 10^8 M_\odot$ black hole at its center (Ferrarese et al. 1996), NGC 4261 is well known for its kiloparsec-scale jets (Birkinshaw & Davies 1985) and its hundred parsec-scale dusty disk imaged by *HST* (Jaffe et al. 1993). This disk possesses an atomic surface density of $\sim 5 \times 10^{20} \text{ cm}^{-2}$, as inferred from its optical depth assuming a Galactic dust/gas ratio. On a smaller scale, a thin circumnuclear disk of radius $\sim 6 \text{ pc}$ was revealed by radio line absorption studies (Jaffe & McNamara 1994; van Langevelde et al. 2000). This portion of the disk has an H I column density of $\sim 2.5 \times 10^{19} T_{\text{sp}} \text{ cm}^{-2}$, where $T_{\text{sp}} \simeq 100 \text{ K}$ is the spin temperature of the gas. At an even smaller scale, free-free absorption of radio emission from the core by a geometrically-thin disk of radius $\sim 0.3 \text{ pc}$ was detected (Jones et al. 1997, 2000, 2001; Piner, Jones & Wehrle 2001). This recent finding adds significant content to the accretion picture because this radius corresponds to only $6400 r_S$, where the Schwarzschild radius $r_S \equiv 2GM/c^2 \simeq 1.45 \times 10^{14} \text{ cm}$ for the central black hole in NGC 4261.

Although these observations of the accretion disk extend to sub-parsec scales, a fully self-consistent accretion model does not yet exist, particularly for the small free-free absorbing disk (Sudou et al. 2000). Jones et al. (2000) did have success in attributing the observed free-free absorption to a standard α -disk. Unfortunately, to match the observations, the model requires a dissipative stress that is much greater than that provided by subsonic turbulence. A viable alternative for (or addition to) this stress must be found in order for the model to be fully self-consistent.

We suggest here that supersonic turbulence is the responsible agent. Observations of NGC 4261 provide direct evidence that turbulence is prominent in the disk from 100 pc to about 6 pc, with the inner boundary set by observational limitations. At 100 pc, the width of narrow lines from the disk suggest a turbulent velocity of 70 km/s (Jaffe et al. 1996), while at 6 pc, the turbulent velocity estimated from the H I absorption profile is about 130 km/s (Jaffe & McNamara 1994; van Langevelde et al. 2000). Strong turbulence in the accretion disk is understandable given that the disk is embedded within the core of the galaxy, where it is subject to disruption by strong stellar winds. The dissipation of turbulence is regulated by the cascade in energy from large scales to small scales, so the total energy associated with the turbulent motion decays roughly as a power-law in time (Lazarian 2003), even in the case of supersonic turbulence (Smith, Mac Low & Zuev 2000a). This slow turbulence decay suggests that the supersonic structure might persist even to

smaller radii.

In such a supersonic disk, the accreting gas is optically-thin and gravitational energy dissipation will overwhelm line cooling at a critical radius r_c , within which the gas is effectively heated to a temperature close to its virial value (Pringle 1981). Thermal pressure of the gas will then dominate the turbulent pressure at $r \simeq (2/3)r_c$, so the supersonic flow appears to terminate at this radius and the gas may make a transition into an advection-dominated accretion flow thereafter (Narayan & Yi 1994). On larger scales, the supersonic structure can be inferred directly from observations. It is interesting to note that with a stress parameter $\alpha \simeq 1$, the value of r_c is roughly 0.3 pc, which corresponds to the inferred size of the free-free absorbing region. Thus the observed shadowing of the nascent radio jet may be produced by the ionized gas near r_c .

We further note that newly released *Chandra* data also hint that the nucleus of NGC 4261 may be weakly-active (Peter, Zezas & Fabbiano 2001), consistent with earlier *ASCA* and *ROSAT* observations (Matsumoto et al. 2001; Worrall & Birkinshaw 1994). The corresponding ionization parameter at 0.3 pc (assuming that the radiation is isotropic) is $\Xi \approx 5$, where $\Xi \equiv F_{\text{ion}} / n_{\text{tot}} k T c$, F_{ion} is the ionizing flux between 1 and 10^3 Ryd, and n_{tot} is the total number density including all species. Note that Ξ roughly corresponds to the ionizing-photon-to-gas pressure ratio. A value of $\Xi \gtrsim 1$ indicates that the gas may be effectively photoionized. This photoionization will significantly affect the profiles of the lines emitted by the supersonic disk. High-resolution *HST* imaging of the central ionized gas has detected broad emission lines from a region smaller than 7 pc in radius (Ferrarese et al. 1996). In this paper, we show that a supersonic disk, irradiated by the AGN, can not only account for the observed radio absorption feature, but also reproduce these broad emission lines. We also show that its large-scale extension is consistent with the radio line absorption observations.

The physical conditions present in the broad line regions (BLRs) of this class of radio galaxy are likely to be very different than those present in the more-luminous Seyfert galaxies and quasars. In both scenarios, the line emission is produced by gas having temperature on the order of a few times 10^4 K, with line broadening caused by bulk motions of the emitting plasma. However, while the BLR in Seyferts and quasars is primarily photoionized, our model predicts that heating due to gravitational dissipation plays a significant role in the low-luminosity radio galaxies.

Our modeling also indicates a very different BLR geometry for these galaxies, with the line emission coming directly from the turbulent accretion disk. While accretion disks may play an important role in some BLR models of Seyferts and quasars, the line emission is not believed to originate in the disk itself, instead being associated with, e.g.,

magnetohydrodynamic flux tubes (Emmering, Blandford, and Shlosman 1992) or radiation- and gas-pressure driven winds rising from the surface of the disk (Murray et al. 1995). The accretion disk does not even play a direct role in many successful BLR models for these objects, e.g., the bloated star (Alexander & Netzer 1994) or accretion-shock cooling models (Fromerth & Melia 2001).

It is also noted that the density of the BLR gas in these galaxies is much lower than in traditional AGNs. Because broad forbidden emission lines are absent in Seyfert and quasar spectra, we know that the density of their line-emitting gas is $n \gtrsim 10^7 \text{ cm}^{-3}$. However, the spectra of some low-luminosity radio galaxies contain strong broad forbidden emission lines (e.g., [N II], [S II]), indicating gas densities $n \lesssim 10^5 \text{ cm}^{-3}$ (see, e.g., Ferrarese & Ford 1999; Barth et al. 1999). The lower density BLR gas may be directly tied to their lower mass accretion rates and resulting luminosities.

We first discuss the general properties of a supersonic disk in § 2. Its consistency with the multi-wavelength observations of NGC 4261 is discussed in § 3. Detailed modeling of the line emission from this supersonic disk, irradiated by its AGN, is given in § 4. In § 5, we discuss the implication of this work on the nature of AGNs in radio galaxies.

2. A Supersonic Accretion Disk Model

Because it is thought that the large-scale dusty disk feeds the inner accretion of the AGN (Jaffe et al. 1996), the detection of a prominent gap in the radio core of NGC 4261 prompted Jones et al. (2000, 2001) to introduce a free-free absorbing disk to account for the observed features. To produce the radio absorption, the inner disk must have an emission measure of $n_e^2 l \simeq 3 \times 10^8 T_4^{3/2} \text{ pc cm}^{-6}$, where n_e is the electron density, l is the path length through the absorbing gas, and T_4 is the electron temperature in units of 10^4 K . If dominated by thermal gas pressure, however, the optically thin α -disk proposed by these authors cannot account for this radio shadowing in a self-consistent manner. In particular, we show below that the implied stress parameter α is too large for the flow to be subsonic.

For a gas-pressure-dominated accretion disk, angular momentum conservation requires that $\nu \simeq -(2/3) v_r r$ at large radii, where $\nu = \alpha H(r) c_s(r)$ is the kinetic viscosity, α is the stress parameter (assumed to be radius-independent and less than one), v_r is the radial velocity of the flow, $H(r)$ is the scale height of the disk, and $c_s(r)$ is the local sound speed. From the expressions given in Jones et al. (2000), one can obtain:

$$\alpha \simeq -\frac{2}{3} \frac{v_r r}{H c_s} = -\frac{2}{3} \frac{v_r}{v_k} \left(\frac{r}{H} \right)^2 = 2.4 \times 10^3 M_8^{1/4} \dot{M}_{-3}^{1/2} r_{18}^{-3/4}, \quad (1)$$

where $v_k = (GM/r)^{1/2}$ is the Keplerian velocity, M_8 is the black hole mass in units of $10^8 M_\odot$, $\dot{M}_{-3} = \dot{M}/(10^{-3} M_\odot/\text{yr})$ gives the accretion rate, and $r_{18} \sim 1$ is the distance of the radio absorbing gas from the black hole in units of 10^{18} cm. In fact, it can be shown that the disk cannot be supported by thermal pressure of the gas alone since the corresponding accretion rate is:

$$\begin{aligned} \dot{M} \simeq & 7.4 \times 10^{19} \alpha \left(\frac{n_o}{2.0 \times 10^5 \text{ cm}^{-3}} \right) \left(\frac{T_o}{10^4 \text{ K}} \right)^{3/2} \\ & \times \left(\frac{M}{4.9 \times 10^8 M_\odot} \right)^{-1} \left(\frac{r_o}{10^{18} \text{ cm}} \right)^3 \text{ g s}^{-1}, \end{aligned} \quad (2)$$

where quantities with subscript o denote the corresponding values inferred from the radio absorption features, and we have approximated the line-of-sight path length through the disk with $2H/\sin(26^\circ)$ (Jones et al. 2001), where $H = (R_g T r^3 / \mu G M)^{1/2}$, R_g is the gas constant and $\mu = 0.5$ is the molecular weight. Such an accretion rate is so small that the implied emission efficiency for converting accreted rest-mass energy into X-ray emission from the nucleus of NGC 4261 is about $3.0/\alpha$ (Worrall & Birkinshaw 1994; Matsumoto et al. 2001), which is unacceptable for any $\alpha \leq 1$ in a thermal pressure supported disk. Sudou et al. (2000) further discussed an optically-thick standard disk and an optically-thin disk cooled by free-free emission. Neither of these alternatives can account for the observed shadowing.

Meanwhile, several observations indicate that turbulence dominates the gas motion at large scales (Jaffe et al. 1996; van Langevelde et al. 2000), where supersonic turbulence may be produced by stellar winds in the core of the galaxy (Jaffe et al. 1996). As the gas falls in toward the black hole, however, the strength of the residual turbulence in the disk is determined by balancing shock dissipation with the turbulence enhancement due to gravitational energy dissipation. In a fully developed turbulent flow, energy is mostly associated with large-scale gas motion. The decay rate of the total turbulent energy is then determined by the rate at which energy cascades from large scales to small scales. The turbulent energy density per unit mass, ε , is therefore given by

$$\dot{\varepsilon} = \varepsilon/\tau, \quad (3)$$

where the dot denotes a derivative with respect to time and $\tau = L/\varepsilon^{1/2}$ gives the characteristic time scale for transporting energy from large to small scales. The characteristic length scale, L , of the system depends on the turbulence generation mechanism. Assuming L is independent of time, we have $\varepsilon \propto t^{-2}$. In their numerical simulations of the decay of supersonic turbulence, Smith et al. (2000a) found that the total energy of the turbulence decays roughly with a power law in time, with an index -1.5 .

We point out that as the large-scale supersonic gas flows inward, the dissipative stress is provided primarily by its turbulent motion. So the dissipated gravitational energy will go first into producing turbulence. This turbulence generation mechanism can, in principle, keep the disk supersonic even on smaller scales (Smith, Mac Low & Heitsch 2000b). A complete model addressing the evolution of this supersonic accretion flow, however, would require a detailed numerical simulation beyond the scope of this paper.

In the following discussion, we will assume that the energy associated with the turbulent motion is in sub-equipartition with, and proportional to, the gravitational energy of the gas. We therefore have

$$v_t^2 = f v_k^2, \quad (4)$$

where f is a “turbulence parameter”, which can be fixed by the observed disk properties at large radii, and v_t is the turbulent velocity in the flow. The supersonic disk model (in which the stress is dominated by turbulence) then gives:

$$\nu = \alpha H v_t, \quad (5)$$

$$H = f^{1/2} r, \quad (6)$$

$$v_r = -1.5 \frac{\nu}{r} = -1.5 \alpha f v_k, \quad (7)$$

$$\dot{M} = 6\pi \alpha f^{3/2} r^2 v_k n m_p. \quad (8)$$

In Eq. (8), $n(r)$ is the baryon number density averaged in the vertical direction of the accretion disk and m_p is the proton mass. Because the H I absorption feature indicates that $v_t \simeq 0.21 v_k$ at $r \simeq 6$ pc from the nucleus, we obtain $f \simeq 0.045$. The corresponding disk opening angle is $2 \tan^{-1} f^{1/2} \simeq 24^\circ$. Then from Equations (6) and (8), we have

$$H = 0.21 r, \quad (9)$$

$$n = n_o \left(\frac{r_o}{r} \right)^{3/2}. \quad (10)$$

It is interesting to note that the viscous time scale in such a disk ($t_{vis} = r/v_r$ by definition) is longer than the corresponding dynamical time scale ($t_d = 2\pi r/v_k$) by a factor of $2.4/\alpha$. Adopting the power-law decay rate from the numerical simulations (Smith et al. 2000a), one can show that the ratio of the turbulent energy to the dissipated gravitational energy is about $0.27\alpha^{3/2}$. This is consistent with $f \approx 0.045$ for α less than one.

One should emphasize that only a small fraction ($\sim 4.5\%$) of the dissipated gravitational energy is left to drive the turbulent motion. Most of the dissipated gravitational energy is thermalized via shocks and effectively radiated away. Since we are mostly interested in

regions where the gas is partially ionized, this cooling is dominated by line emission. We will see that there is a critical radius r_c in the disk, where the gravitational energy dissipation rate equals the line cooling rate. The gravitational energy dissipation rate is given by

$$\Gamma = \frac{3}{8\pi} \frac{GM\dot{M}}{Hr^3}. \quad (11)$$

From Equation (8), we have

$$\begin{aligned} \dot{M} &= 2.3 \times 10^{24} \alpha \left(\frac{f}{0.045} \right)^{3/2} \left(\frac{n_o}{3 \times 10^4 \text{ cm}^{-3}} \right) \\ &\times \left(\frac{r_o}{10^{18} \text{ cm}} \right)^{3/2} \left(\frac{M}{4.9 \times 10^8 M_\odot} \right)^{1/2} \text{ g s}^{-1}. \end{aligned} \quad (12)$$

Using this equation to eliminate \dot{M} in Equation (11), we get

$$\begin{aligned} \Gamma &= 8.5 \times 10^{-14} \alpha \left[\left(\frac{f}{0.045} \right) \left(\frac{n_o}{3 \times 10^4 \text{ cm}^{-3}} \right) \left(\frac{r_o}{10^{18} \text{ cm}} \right)^{3/2} \right. \\ &\times \left. \left(\frac{r}{10^{18} \text{ cm}} \right)^{-4} \left(\frac{M}{4.9 \times 10^8 M_\odot} \right)^{3/2} \right] \text{ ergs cm}^{-3} \text{ s}^{-1}. \end{aligned} \quad (13)$$

The line cooling rate of an optically-thin gas is given by

$$\begin{aligned} \Lambda \equiv n^2 \lambda &= 9.0 \times 10^{-14} \lambda_{-22} \left[\left(\frac{n_o}{3 \times 10^4 \text{ cm}^{-3}} \right)^2 \right. \\ &\times \left. \left(\frac{r_o}{10^{18} \text{ cm}} \right)^3 \left(\frac{r}{10^{18} \text{ cm}} \right)^{-3} \right] \text{ ergs cm}^{-3} \text{ s}^{-1}, \end{aligned} \quad (14)$$

where λ is the cooling function (Krolik 1999) and $\lambda_{-22} \equiv \lambda/(10^{-22} \text{ ergs cm}^3 \text{ s}^{-1})$.

In terms of the critical radius r_c , we have

$$\begin{aligned} \alpha \left(\frac{f}{0.045} \right) \left(\frac{M}{4.9 \times 10^8 M_\odot} \right)^{3/2} &= 1.06 \lambda_{-22} \left(\frac{n_o}{3 \times 10^4 \text{ cm}^{-3}} \right) \\ &\times \left(\frac{r_o}{10^{18} \text{ cm}} \right)^{3/2} \left(\frac{r_c}{10^{18} \text{ cm}} \right). \end{aligned} \quad (15)$$

To account for the radio shadowing, the electron number density should be $\sim 3 \times 10^4 \text{ cm}^{-3}$ at $\sim 0.3 \text{ pc}$, where we have assumed an inclination angle $i = 64^\circ$ for the disk (Jones et al. 2001). Thus, for a stress parameter $\alpha \simeq 1$, Equation (15) shows that the critical point is located within the radio shadowing region. It is natural to expect that the observed radio absorption should be produced by the fully ionized gas near r_c , and we will see below that

ionizing photons from the central engine play a crucial role in determining the ionization state of the gas at this radius.

HST observations indicate that the gas closest to the nucleus may be ionized by radiation from the central engine (Ferrarese et al. 1996). Further evidence for this can be shown by estimating the ionization parameter at r_c . Recent high-resolution *Chandra* observations have uncovered a high-energy source at the nucleus of NGC 4261 with a hard band X-ray luminosity of $L \approx 7 \times 10^{40}$ ergs/s (Peter et al. 2001), confirming earlier *ASCA* results (Matsumoto et al. 2001). Meanwhile, the soft X-ray luminosity is $\sim 10^{41}$ ergs/s (Worrall & Birkinshaw 1994). So, assuming that the radiation is isotropic and that the gas temperature is $\sim 10^4$ K, we can estimate the value of the ionization parameter to be $\Xi \simeq 5$ for the radio-absorbing gas at $\sim 10^{18}$ cm (Krolik 1999). The radio-absorbing gas is therefore effectively photoionized.

Although the radiation pressure dominates the thermal pressure of the gas in the radio absorbing region, the turbulent pressure there is $0.5 n_o m_p v_t^2 \simeq 7.4 \times 10^{-5}$ ergs cm^{-3} , which is much larger than the radiation pressure. So the disk structure, including the scale height and number density, is still determined by the turbulent motion. However, the gas temperature profile depends on the interaction between the disk and the radiation field. In the following sections, we will incorporate this photoionization effect using the algorithm Cloudy (Ferland 1996; Cloudy 96- $\beta 3$) and show that the observed broad-line spectrum may also be fitted with this disk model in a self-consistent fashion.

3. Line Emission from the Irradiated Supersonic Disk

To model line emission from the irradiated disk, we first need to know the intensity and spectral energy distribution (SED) of the ionizing radiation from the central source. These are highly uncertain due to a combination of factors. First, there are uncertainties associated with intrinsic absorption and galactic contamination which limit the precision to which we can quantify the spectrum in the optical and X-ray bands. Second, the spatial distribution of photons is unknown — it is unclear whether the central engine emits isotropically; the disk at r_c may “see” a different spectrum from what we observe. Third, and most importantly, we do not have observations (or even good estimates) of the continuum at UV energies. Generally, the shape and intensity of the UV continuum most strongly determine the properties of a photoionized gas.

The correlations between radio and optical spectra have suggested a non-thermal nuclear source for FR I radio galaxies (Chiaberge, Capetti & Celotti 1999). Further

evidence for a power-law nuclear source in NGC 4261 comes from *ROSAT* and *ASCA* observations in the X-ray band (Worrall & Birkinshaw 1994; Matsumoto et al. 2001), which are confirmed by recent high spatial resolution *Chandra* observations (Rinn & Sambruna 2001; Peter et al. 2001). In the following discussion, we will adopt a power-law spectrum in the UV-range to bridge the gap between the optical and X-ray data. The continuum is assumed to be emitted isotropically from a central, point-like source, and the intensity of the ionizing luminosity remains a free parameter in our model to reflect our uncertainties.

We are mostly interested in the region at ~ 0.3 pc. However, to determine the spectrum of the incident radiation, we also need to know the gas distribution in the inner region since radiation from the core may be reprocessed by intermediate gases. Fortunately, according to the supersonic disk model, the disk will be heated up very quickly within r_c , which makes the gas there optically-thin to UV and X-ray emission. One can show this by solving the energy conservation equation in the transition region between r_c and the radius r_t , where the thermal pressure of the gas equals the turbulent pressure and the supersonic accretion flow effectively terminates.

For a supersonic accretion disk, we have the energy conservation equation:

$$\frac{d}{dr} \left[1.5 (1 - f) \dot{M} v_k^2 - \frac{5 \dot{M} k_B T}{m_p} \right] = -4\pi r H \Lambda . \quad (16)$$

The first term on the left-hand side corresponds to the gravitational energy dissipation and turbulent advection, while the second term is associated with the thermal energy of the gas. The right-hand side gives the cooling. The quantity $\Lambda/n^2 \equiv \lambda$ is about 10^{-22} ergs $\text{cm}^3 \text{s}^{-1}$ near the peak (at $\sim 10^4$ K) of the cooling function (Krolik 1999). Assuming that λ does not depend on radius, we have the following temperature profile in the transition zone:

$$\begin{aligned} T(r) &= T_c + \frac{0.3 (1 - f) G M}{r_c R_g} \left[\frac{r_c}{r} - 1 + \ln(r/r_c) \right] \\ &\simeq T_c + \frac{0.15 (1 - f) G M}{r_c R_g} \left[\frac{r_c - r}{r} \right]^2 \\ &= T_c + 1.2 \times 10^8 (1 - f) \left(\frac{r_c - r}{r} \right)^2 \\ &\quad \left(\frac{r_c}{10^{18} \text{ cm}} \right)^{-1} \left(\frac{M}{4.9 \times 10^8 M_\odot} \right) \text{ K} . \end{aligned} \quad (17)$$

In the second expression above, we have kept only the term proportional to $[(r_c - r)/r]^2$ and have neglected the high order terms in $(r_c - r)/r$. Setting $2 k_B T(r_t) = f m_p v_k^2$, we obtain the termination radius r_t of the supersonic flow:

$$r_t = \frac{r_c}{1 + a/2 + (a + a^2/4)^{1/2}} , \quad (18)$$

where

$$a = \frac{f}{0.3(1-f)} \simeq 0.15 \left(\frac{f}{0.045} \right). \quad (19)$$

So $r_t \simeq (2/3)r_c$, and $T(r_t) \simeq 3 \times 10^7$ K. Then the error introduced by neglecting the high order terms in Equation (17) is $\sim 30\%$. In general, the termination radius r_t is determined by solving the equation

$$\ln \left(\frac{r_t}{r_c} \right) = 1 + \frac{(8f-3)r_c}{3(1-f)r_t}. \quad (20)$$

So f must be smaller than $3/8$ to make the thermal pressure of the gas dominate at small radii. A larger value of f will cause the turbulent advection to cancel most of the gravitational energy dissipation and keep the disk supersonic. In addition, a more accurate expression for λ in the transition zone will make the gas heated even faster because it is on the unstable portion of the cooling curve (Liu, Fromerth & Melia 2002). Within r_t , the accretion pattern may transfer into an advection dominated flow (Narayan & Yi 1994).

Within r_c , the disk is optically-thin to UV and X-ray radiation, and because of the sharp increase in the gas temperature in this region, free-free absorption is also negligible. Due to the effects of photoionization by the AGN, however, the gas will be fully ionized well beyond r_c . To incorporate this effect self-consistently, we will need to use the algorithm Cloudy with additional heating introduced by gravitational dissipation to calculate the temperature and the ionization state of the gas everywhere in the disk.

Before calculating the line emission from the supersonic disk numerically, it may be illustrative to estimate the physical conditions of the broad-line region. Observations with *HST* have identified an ionized gas concentration in a spatially-resolved region with a FWHM of 17 pc. The broad emission lines are associated with the central $0''.1 \sim 14$ pc aperture position (Farrase et al. 1996). For the $H\alpha$ line, the observed flux is 3.11×10^{-15} ergs cm^{-2} s^{-1} with a FWHM of 2500 km/s. From the electron number density inferred above and the $H\alpha$ volume emissivity of $\sim 2 \times 10^{-25}$ ergs cm^3 s^{-1} (Osterbrock 1974), we can estimate the size of the emission region. In our model, most of the lines should be produced beyond r_o . The radius r of this region should therefore satisfy the condition

$$4.8 \times 10^{38} \left(\frac{f}{0.045} \right)^{-1/2} \left(\frac{n_o}{3 \times 10^4 \text{ cm}^{-3}} \right)^2 \left(\frac{r_o}{10^{18} \text{ cm}} \right)^3 \ln(r/r_o) = 3.3 \times 10^{38}, \quad (21)$$

implying that $r \approx 0.6$ pc. It is interesting to note that the Keplerian velocity at such a radius is 1900 km/s, which is consistent with the FWHM of the $H\alpha$ line if one takes into account the turbulent motion in the flow and the inclination of the disk. Because the contributions to $H\alpha$ from the various rings at different radii are comparable to each other between ~ 0.3 pc and ~ 0.6 pc, the double peaks that are usually produced by Keplerian

motion are here filled in, consistent with the observed spectrum. So a supersonic accretion disk with the properties described above appears to account for the broad emission lines rather naturally.

4. Modeling the Broad Emission-Line Spectrum

Several observational constraints already limit the parameter space available for fitting the broad emission lines. Images from *HST* show that the large-scale dusty disk has an inclination angle of 64° (Jaffe et al. 1993). On the other hand, the narrow-line kinematic data from the central region suggests an inclination angle of 69° for the ten-parsec scale disk. Both of these values are consistent with the viewed angle of the radio jet, which is $\sim 63^\circ$ (Piner et al. 2001). We therefore adopt a value of $i = 64^\circ$ for the inclination angle of the supersonic disk.

As stated in Section 2, the radio-line absorption observations fix the turbulent parameter at $f = 0.045$. To account for the radio shadowing near 0.3 pc, the electron number density should be around $30,000 \text{ cm}^{-3}$. Because we expect hydrogen to be fully ionized in this region, we will choose $n_o = 30,000 \text{ cm}^{-3}$ as the fiducial value for the scale-height-averaged number density of the disk at a radius $r_o = 10^{18} \text{ cm}$ from the supermassive black hole. The remaining free parameters in the model are the ionizing luminosity L_{ion} , and the stress parameter α , which determines the accretion rate and critical radius via Equations (12) and (15).

4.1. Methodology

We use Cloudy to calculate the line emissivity as a function of radius for $r > r_c$, including the additional heating (Eq. 13) and varying the density with radius (Eq. 10) as predicted by our model. The line profiles are then generated by integrating over the appropriate range in radius. We accomplish this task by partitioning the disk into a large set of concentric tori, modeling the line emission from each torus as a set of N discrete clouds, with the understanding that we approach the continuous limit with very large N . The emission line flux from the population of N clouds in torus i as a function of wavelength is:

$$F_i(r, \lambda) \propto 2\pi r_i H(r_i) \Delta r_i \sum_{j=1}^N \epsilon(\mathbf{r}_j, \mathbf{v}_j) \Lambda(\mathbf{r}_j, \mathbf{v}_j, \lambda) , \quad (22)$$

where the factor $2\pi r_i H(r_i) \Delta r_i$ is the volume of torus i , $\epsilon(\mathbf{r}_j, \mathbf{v}_j)$ is the line emissivity including relativistic effects, and $\Lambda(\mathbf{r}_j, \mathbf{v}_j, \lambda)$ is a convolution term relating a cloud’s location and velocity to the observed line wavelength. The composite line flux from the entire disk is then obtained by summing the contributions from each torus.

Taking the line-of-sight velocity to be v_{los} , the effect of Doppler boosting is given by (Corbin 1997):

$$\epsilon(\mathbf{r}, \mathbf{v}) = \epsilon_0(\mathbf{r}) \left(\frac{\sqrt{1 - v^2/c^2}}{1 + v'_{\text{los}}/c} \right)^3, \quad (23)$$

where $\epsilon_0(\mathbf{r})$ is the rest-frame emissivity (generated by Cloudy) and

$$v'_{\text{los}} = v_{\text{los}} + c \left(\sqrt{1 - \frac{r_S}{r}} - 1 \right) \quad (24)$$

is the line-of-sight velocity including general-relativistic corrections.

The observed wavelength λ of line emission from a given cloud is related to rest-frame line wavelength λ_0 by

$$\lambda = \lambda_0 \left(1 - \frac{r_S}{r} \right)^{-1/2} \left(\frac{\sqrt{1 - v^2/c^2}}{1 - v_{\text{los}}/c} \right) (1 + z), \quad (25)$$

where the correction terms on the right are the gravitational, Doppler, and cosmological redshifts, respectively. This relation, appearing as a delta-function $\Lambda(\mathbf{r}_j, \mathbf{v}_j, \lambda)$ in Eq. (22), is used to map each cloud’s emission into predetermined wavelength bins.

The axis of the disk is taken to lie along the z -axis. Cloud positions and velocities are then determined via Monte Carlo sampling. Each cloud is given a random azimuthal position $0 \leq \phi < 2\pi$ in the disk, and the velocity of each cloud is assigned according to

$$\mathbf{v}_j = v_k \mathbf{n}_\phi + \mathbf{v}_t, \quad (26)$$

where $v_k = (GM/r)^{1/2}$ is the Keplerian velocity, \mathbf{n}_ϕ is the azimuthal direction vector (note that this depends on the value of ϕ), and $\mathbf{v}_t = \sqrt{f} v_k$ in a randomly-oriented direction. The line-of-sight velocity is then equal to $v_{\text{los}} = \mathbf{v}_j \cdot \mathbf{n}_{\text{los}}$, where \mathbf{n}_{los} is the direction vector along the line of sight.

4.2. Results of the Line Modeling

We have modeled the continuum-subtracted H α $\lambda 6563 + [\text{N II}] \lambda \lambda 6548, 6584$ and [S II] $\lambda \lambda 6717, 6731$ broad emission-line spectrum of Ferrarese et al. (1996). The parameters

L_{ion} and α were varied to determine the best χ^2 fit to their nuclear pixel data, corresponding to a FWHM spatial resolution of $\theta'1 = 14$ pc. Figure 1 shows the resulting best fit ($\chi^2_{\nu} = 1.1$; $\nu = 250$ degrees of freedom), having parameters $L_{\text{ion}} = 4 \times 10^{40}$ erg/s and $\alpha = 0.4$. The model nicely reproduces the broad wings and steep core of the H α + [N II] composite. There is an apparent excess in the modeled [S II] emission, which may be remedied by reducing the assumed abundance of sulfur in the model (we used solar abundances throughout). Allowing for this additional free parameter is beyond the scope of this paper, however, as we are more interested in showing a consistency in the line profiles rather than their relative strengths.

Figure 2 shows the radial dependence of the gas temperature and the ionization fraction of hydrogen in the best fit model. From this we see that most of the hydrogen is ionized near 1 pc from the center. So significant free-free absorption is expected in the region.

Thermal equilibrium occurs when the heating and cooling rates balance; stable equilibria occur only where the slope of the cooling function is positive (e.g., Shore 1992). Figure 3 illustrates the heating and cooling functions for the gas at radii $r = 10^{17}$ cm (top) and $r = 10^{20}$ cm (bottom). The heating rate includes both gravitational dissipation and radiative effects, and the cooling rate must be determined including the dependency on the ionization state of the gas. Cloudy calculates both of these rates in a self-consistent manner. At $r = 10^{17}$ cm, it is clear that only one stable solution exists, $T \simeq 10^5$ K (compare with Fig. 2), so there is no ambiguity in determining the equilibrium temperature. At large radii, however, it is apparent that two valid physical solutions exist. Because our picture has the gas being heated from a low temperature as it accretes, we assign the smaller value in all such cases of uncertainty. As shown in figure 2, the gas temperature jumps from $\sim 2 \times 10^3$ K to $\sim 10^4$ K near 4×10^{19} cm when the gas moves from the lower temperature stable branch to the higher temperature one. This is interesting because neutral atomic hydrogen is concentrated at that radius and this may therefore explain the detected neutral hydrogen radio line absorption.

We have shown that our model can reproduce the observed broad-line spectrum; we now turn to the question concerning the observed absorption features. The free-free absorption optical depth at frequency ν is given by (Walker et al. 2000):

$$\tau_{\nu}^{\text{ff}} = (9.8 \times 10^{-3}) n_e^2 l T^{-1.5} \nu^{-2} \left[17.7 + \ln(T^{1.5} \nu^{-1}) \right], \quad (27)$$

where all the quantities are given in cgs units. The line-center H I $\lambda 21$ cm optical depth, corrected for stimulated emission, is given by (Rohlf, Wilson, & Huettemeister 2000):

$$\tau_0^{21 \text{ cm}} = \left(1.45 \times 10^{-15} \text{ cm}^2 \text{ Hz K} \right) \frac{N_H}{\Delta \nu_D T}, \quad (28)$$

where N_H is the neutral hydrogen column depth and

$$\Delta\nu_D = \frac{1}{\lambda} \sqrt{\frac{2kT}{m_H} + v_t^2} \quad (29)$$

is the Doppler line width (including both turbulent and thermal broadening). Note that for $r > r_c$, the turbulent velocity of the gas is always much greater than the thermal velocity. Figure 4 shows the radial dependence of both of these optical depths for our best-fit model, under the assumption that the line of sight is perpendicular to the disk. The free-free absorption is strong enough to account for the observed radio shadowing. However, the neutral hydrogen absorption seems deficient. This is not surprising given that we have neglected the density contrast of the supersonic disk in the calculation. Observations of other radio galaxies have revealed that the gas is clumpy at the same spatial scale (e.g., Harms et al. 1994; Haschick, Baan & Peng 1994; Kartje, Königl & Elitzur 1999). Introducing density contrast will not only change the temperature profile of the gas, but also increase the neutral hydrogen column density. So we would expect significant enhancement of radio line absorption in a detailed modeling that incorporates these additional effects.

Figure 5 illustrates how the ionizing flux modifies the line spectrum. With an increase in L_{ion} , the heating and ionization parameters of the gas increase as well. This has the effect of moving the emission zone to larger radii, particularly for the low ionization [N II] and [S II] species. As a result, the line profiles become narrower for increasing L_{ion} . A reduction of L_{ion} from the best fit value does not have such a drastic impact, however. This is because the inner radius reaches an asymptotic limit in the low luminosity case, determined solely by balancing the gravitational heating and line cooling rates via Equation (15). In this limit, the additional heating due to the radiation field is negligible. It is interesting to note that our best fit lies on the transition to this limit.

The dependence of the line shape on the stress parameter α is demonstrated in Fig. 6. A larger α increases the accretion rate (for a fixed number density at r_o), causing additional heating in the gas (via Eq. 13). This moves the emission zone to larger radii, resulting in narrower line profiles. Decreasing α has the opposite effect.

We have used the observed radio free-free absorption to fix our value of n_o in the best fit model. Figure 7 illustrates the effect of varying n_o . The density of the gas is important in many aspects, including a determination of the ionization parameter, as well as the gravitational heating and line cooling rates. It also has a strong impact on the fluxes of the [SII] and [NII] forbidden lines, which are suppressed relative to $H\alpha$ for densities greater than the critical density, at which the radiative and collisional transition rates balance.

Because the line emission broadening is due mainly to the Keplerian motion of the

gas, the line width is proportional to $v_k \sin i$, where v_k is the Keplerian velocity in the disk. The projection effect, characterized by the inclination angle i , is demonstrated in Fig. 8. As expected, model spectra associated with small inclination angles have very narrow line profiles. Note, however, that even when $i = 0$ the lines have non-zero width. This is the effect of broadening due to the turbulent velocity $v_t = \sqrt{f}v_k$.

Finally, the turbulent parameter f has a similar effect on the accretion rate as the stress parameter α . However, by increasing f , we not only shift the broad emission line region toward large radii, but also increase the total line flux, as the disk becomes thicker (thereby increasing the size of the emission region). Figure 9 shows how the line spectrum changes with f .

5. Discussion

The accretion flow within r_t is not well constrained. The fact that the inferred accretion rate from this supersonic disk model gives a radiative efficiency of $\sim 2 \times 10^{-4}$ suggests that advection may dominate in the inner region (Narayan & Yi, 1994). However, if we associate the observed X-ray emission with such an advection dominated accretion flow (ADAF) at small radii, we find that the observed X-ray spectrum with a spectral index of ~ 0.4 (Rinn & Sambruna 2001; Matsumoto et al 2001) is somewhat softer than that of the model prediction (Narayan et al. 1998). An ADAF with strong winds may be able to produce a softer X-ray spectrum to account for the high energy emission from the AGN in NGC 4261 (Quataert & Narayan 1999). And this outflow may be associated with the jet formation process in the core.

It is also interesting to note that NGC 6251 is quite similar to NGC 4261 in that both of them have a hundred-pc scale dusty disk, large scale symmetric radio jets and an inverted radio spectrum at the core (Melia, Liu & Fatuzzo 2002). Compared with NGC 4261, NGC 6251 is about 3 times further away from us, its X-ray luminosity is 30 times stronger, and its broad $H\alpha$ line flux is about 100 times bigger. HST observations suggest that there is a supermassive black hole of $6 \times 10^8 M_\odot$, which is very close to the black hole mass in NGC 4261. If a similar accretion flow exists in NGC 6251, Equation (21) suggests that the electron number density must increase by a factor of ~ 10 to produce the strong $H\alpha$ emission. Combining this with the fact that the disk has an inclination angle of $\sim 32^\circ$ (Ferrarese & Ford 1999) and that the AGN is more active, we would expect that the observed broad emission line may also be fitted with our model. We also would expect strong radio line absorption in the direction of the counterjet with an H I column density of $\sim 10^{23} \text{ cm}^{-2}$.

In an earlier paper we introduced a hot expanding gas model for the multi-wavelength spectrum of the AGN in NGC 6251 (Melia et al. 2002). According to that picture, a standard α -disk with an accretion rate of $\sim 4 \times 10^{22} \text{ g s}^{-1}$ exists near the black hole. How such a fossil disk can form after the supersonic disk terminates is still an open question. However, the implied strong evaporation of the accretion flow below r_t suggests another origin for the hot unbound gas proposed in that model. Further investigation is clearly warranted, and an application of the supersonic disk model to other radio galaxies may also prove to be invaluable in developing a unified theory for supermassive black hole accretion.

Acknowledgments

This research was partially supported by NASA under grants NAG5-8239 and NAG5-9205, and has made use of NASA’s Astrophysics Data System Abstract Service. FM is very grateful to the University of Melbourne for its support (through a Miegunyah Fellowship). MJF would like to thank Gary Ferland for his helpful suggestions.

REFERENCES

- Alexander, T. & Netzer, H. 1994, *MNRAS*, **270**, 781.
- Birkinshaw, M., & Davies, R.L. 1985 *ApJ*, 291, 32
- Chaiberge, M., Capetti, A., & Celotti, A. 1999, *A&A*, 349, 77
- Collin, S., & Huré, J.-M. 1999, *A&A*, 341, 385
- Corbin, M. R. 1997, *ApJ*, 485, 517
- Emmering, R. T., Blandford, R. D., & Shlosman, I. 1992, *ApJ*, 385, 460
- Ferland, G. J. 1996, “Hazy, a Brief Introduction to Cloudy”, University of Kentucky Department of Physics and Astronomy Internal Report
- Ferrarese, L., Ford, H.C., & Jaffe, W. 1996, *ApJ*, 470, 444
- Ferrarese, L., & Ford, H.C. 1999, *ApJ*, 515, 583
- Fromerth, M.J., & Melia, F. 2001, *ApJ*, 549, 205
- Gaetz, T.J., & Salpeter, E.E., 1983, *ApJS*, 52, 155
- Ho, L. 1999, *ApJ*, 516, 672

- Hubeny, I. 1990, *ApJ*, 351, 632
- Huré, J.-M., Collin-Souffrin, S., Bourlot, J.Le, & des Forêts, G. Pineau 1994, *A&A*, 290, 19
- Jaffe, W., Ford, H.C., Ferrarese, L., van den Bosch, F., & O’Connell, R.w. 1993, *Nature*, 364, 213
- Jaffe, W., & McNamara, R. 1994, *ApJ*, 434, 110
- Jaffe, W., Ford, H.C., Ferrarese, L., van den Bosch, F., & O’Connell, R.w. 1996, *ApJ*, 460, 214
- Jones, D.L., & Wehrle, A.E. 1997, 484, *ApJ*, 186
- Jones, D.L., Wehrle, A.E., Meier, D.L., & Piner, B.G. 2000, *ApJ*, 534, 165
- Jones, D.L., Wehrle, A.E., Meier, D.L., & Piner, B.G. 2001, *ApJ*, 553, 968
- Krolik, J. H., McKee, C. F. & Tarter, C. B. 1981, *ApJ*, 249, 422
- Krolik, J.H. 1999, *Active Galactic Nuclei* (Princeton University Press)
- Lazarian, A. 2003, private communication
- Liu, S., Fromerth, M., & Melia, F. 2002, *ApJ*, 565, 952
- Maloney, P.R., Hollenbach, D.J., & Tielens, A.G.G.M. 1996, *ApJ*, 466, 561
- Matsumoto, Y., Fukazawa, Y., Nakazawa, K., Iyomoto, N., & Makishima, K. 2001, *PASJ*, 53, 475
- Melia, F. & Falcke, H. 2001, *ARAA*, 39, 309
- Melia, F., Liu, S., & Fatuzzo, M. 2002, *ApJ*, 567, 811
- Murray, N., Chiang, J., Grossman, S. A., & Voit, G. M. 1995, *ApJ*, 451, 498
- Narayan, R., & Yi, I. 1994, *ApJ*, 428, L13
- Narayan, R., Mahadevan, R., Grindly, J.E., Popham, R., & Gammie, C. 1998, *ApJ*, 492, 554
- Osterbrock, D.E. 1974, *Astrophysics of Gaseous Nebulae* (San Francisco: Freeman)
- Peter, A., Zezas, A., & Fabbiano, G. 2001, *AAS*, 199, 9908P

- Piner, B.G., Jones, D.L., & Wehrle,, A.E. 2001, AJ, 122, 2954
- Pollack, J.B., Hollenbach, D., Beckwith, S., Simonelli, D.P., Roush, T., & Fong, W. 1994, ApJ, 421, 615
- Pringle, J.E. 1981, ARA&A, 19, 137
- Quataert, E., & Narayan, R. 1999, ApJ, 520, 298
- Rohlfs, K., Wilson, T. L., & Huettemeister, S. 2000, Tools of radio astronomy (Berlin: Springer)
- Rinn, A., & Sambruna, R.M. 2001, AAS, 199, 51111R
- Shakura, N.I., & Sunyaev, R.A. 1973, A&A, 24, 337
- Shore, S. N. 1992, An Introduction to Astrophysical Hydrodynamics (San Diego: Academic Press)
- Smith, M.D., Mac Low, M.-M., & Zuev, J.M., 2000a, A&A, 356, 287
- Smith, M.D., Mac Low, M.-M., & Heitsch, F., 2000b, A&A, 362, 333
- Sudou, H., et al. 2000, PASJ, 52, 989
- van Langevelde, H.J., Pihlström, Y.M., Conway, J.E., Jaffe, W., & Schilizzi, R.T. 2000, A&A, 354, L45
- Worrall, D.M., & Birkinshaw, M. 1994, ApJ, 427, 134

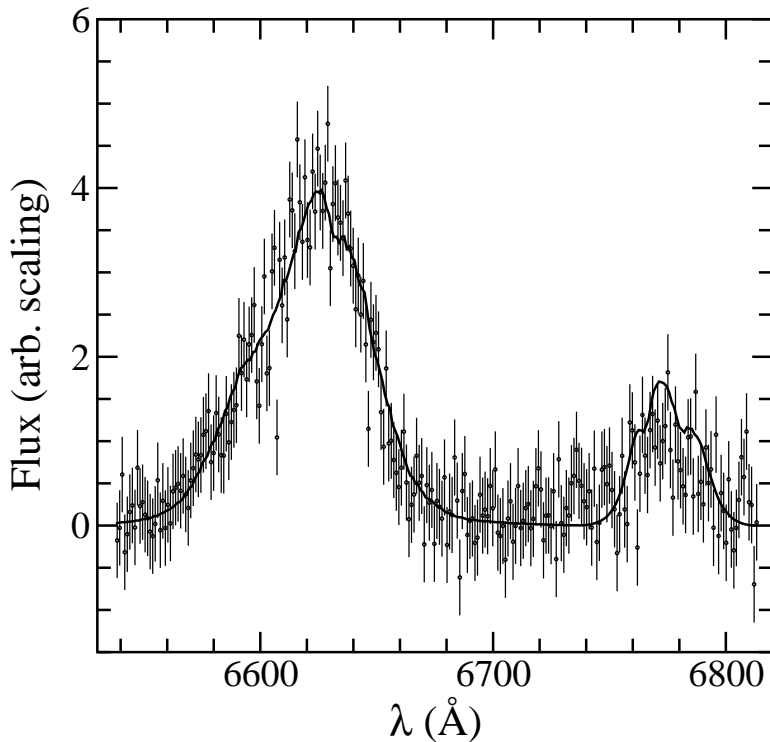


Fig. 1.— Observed (points with error bars) and best-fit modeled (solid curve) broad optical line spectrum of NGC 4261. The best-fit free parameters are $L_{\text{ion}} = 4 \times 10^{40}$ erg/s and $\alpha = 0.4$, resulting in $\chi^2_\nu = 1.1$ ($\nu = 250$ degrees of freedom). The other parameters are fixed in the fit: $n_o = 30000 \text{ cm}^{-3}$, $f = 0.045$, and $i = 64^\circ$ (see text for details).

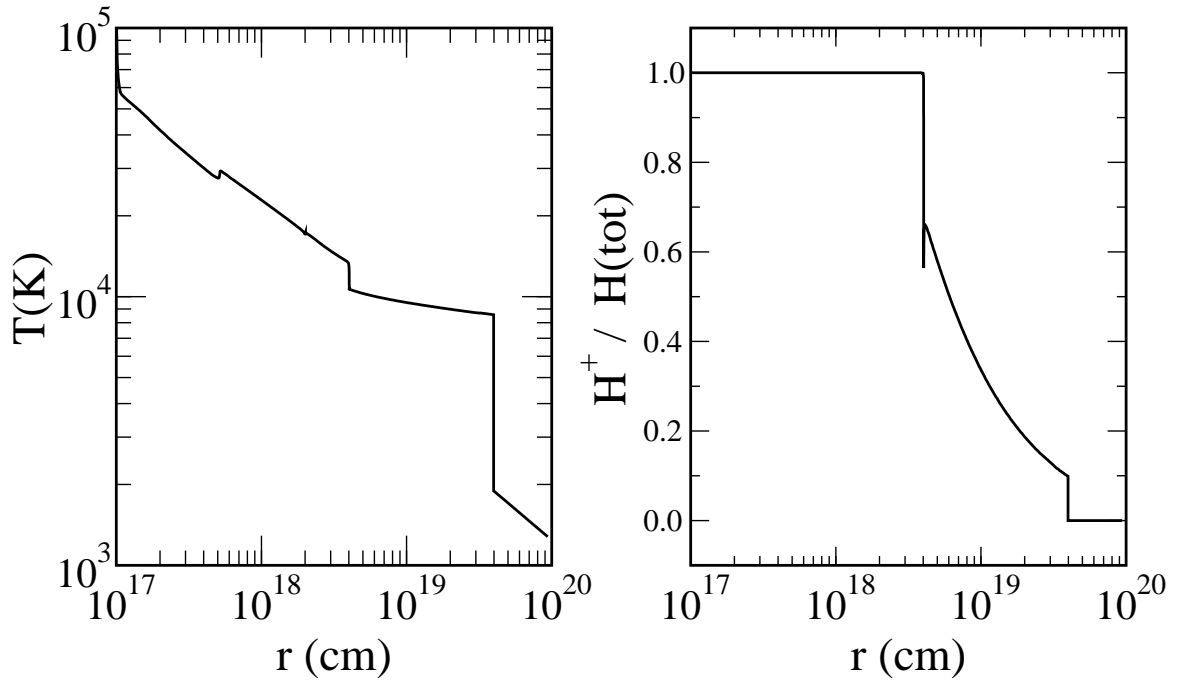


Fig. 2.— The electron temperature (left) and ionization fraction (right) profiles of the disk.

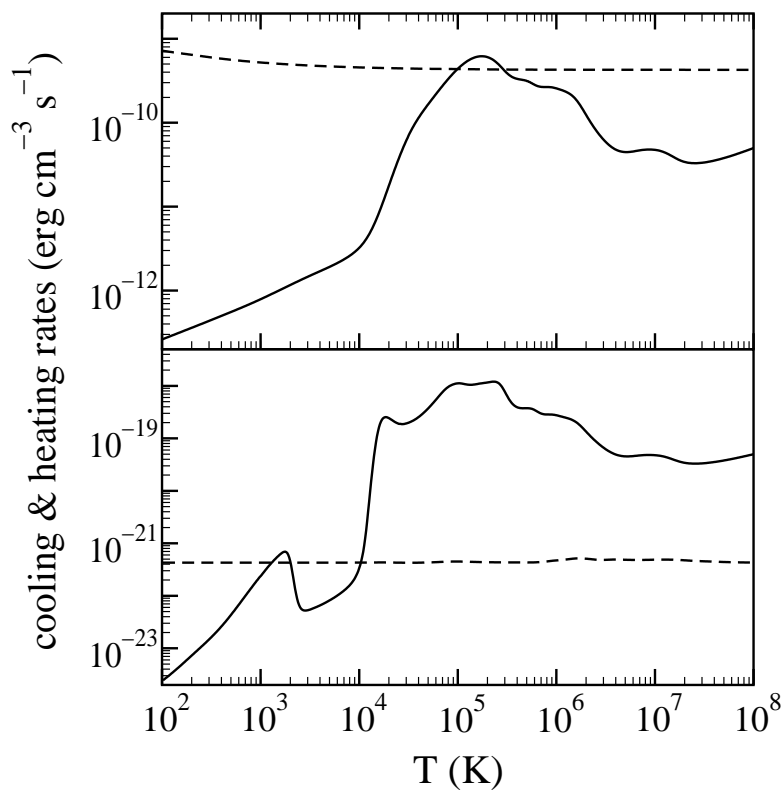


Fig. 3.— Cooling (solid curves) and heating (dashed curves) rates in the disk gas at $r = 10^{17}$ cm (top) and $r = 10^{20}$ cm (bottom). Note that the equilibrium temperature occurs where the heating and cooling rates balance. Stable equilibria occur only where the slope of the cooling function is positive. See text for details.

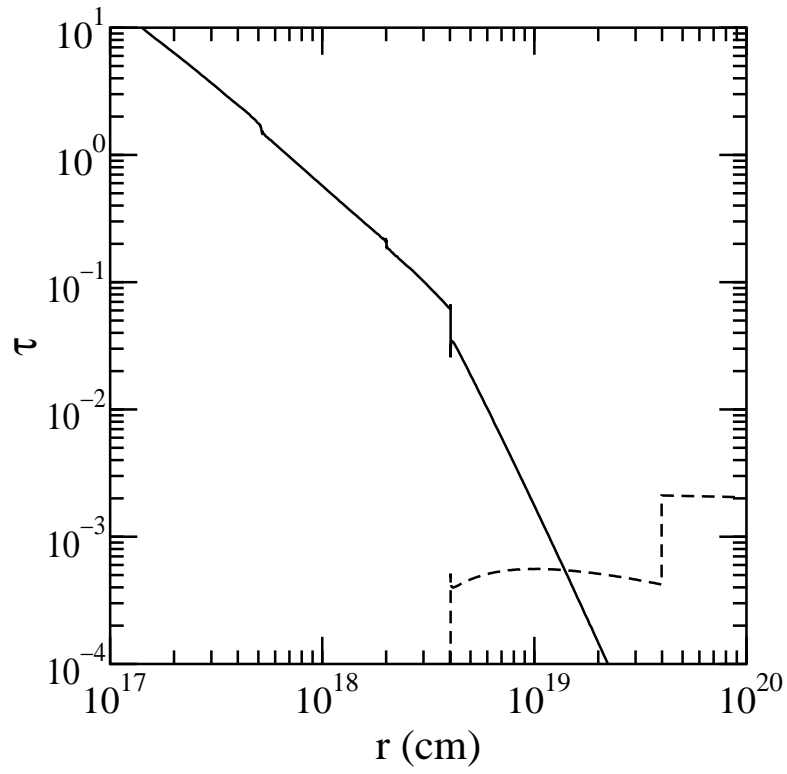


Fig. 4.— The free-free optical depth τ_{ν}^{ff} at 5 GHz (solid curve) and the line-center optical depth $\tau_0^{21\text{cm}}$ of H I $\lambda 21$ cm (dashed curve), calculated for the supersonic disk viewed face-on.

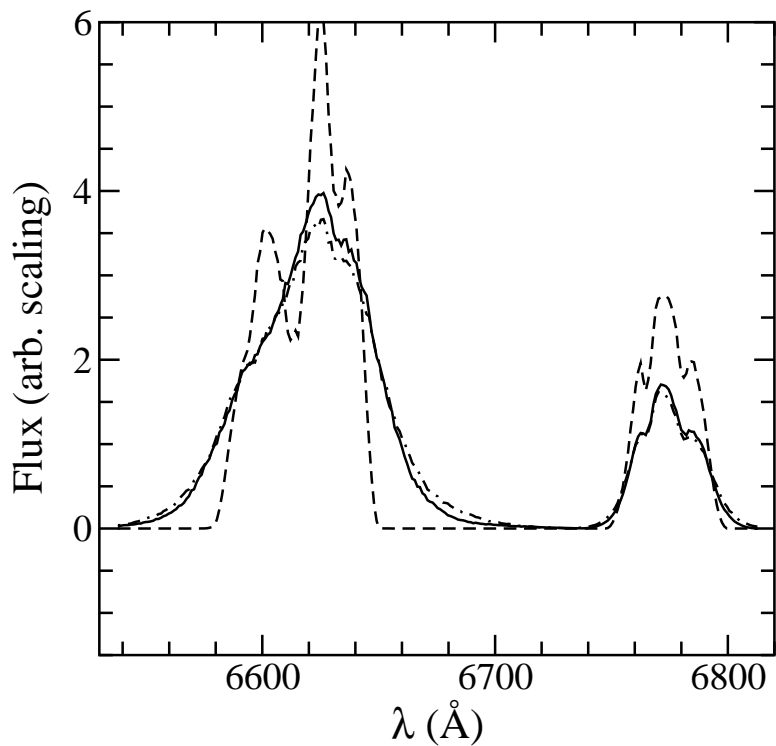


Fig. 5.— The dependence of the broad-line spectrum on the ionizing luminosity L_{ion} . Shown in the figure are the modeled spectra for $L_{\text{ion}} = 4 \times 10^{39}$ erg/s (dot-dashed curve), $L_{\text{ion}} = 4 \times 10^{40}$ erg/s (solid curve), and $L_{\text{ion}} = 4 \times 10^{41}$ erg/s (dashed curve). The other parameters are fixed at: $\alpha = 0.4$, $n_o = 30000 \text{ cm}^{-3}$, $f = 0.045$, and $i = 64^\circ$.

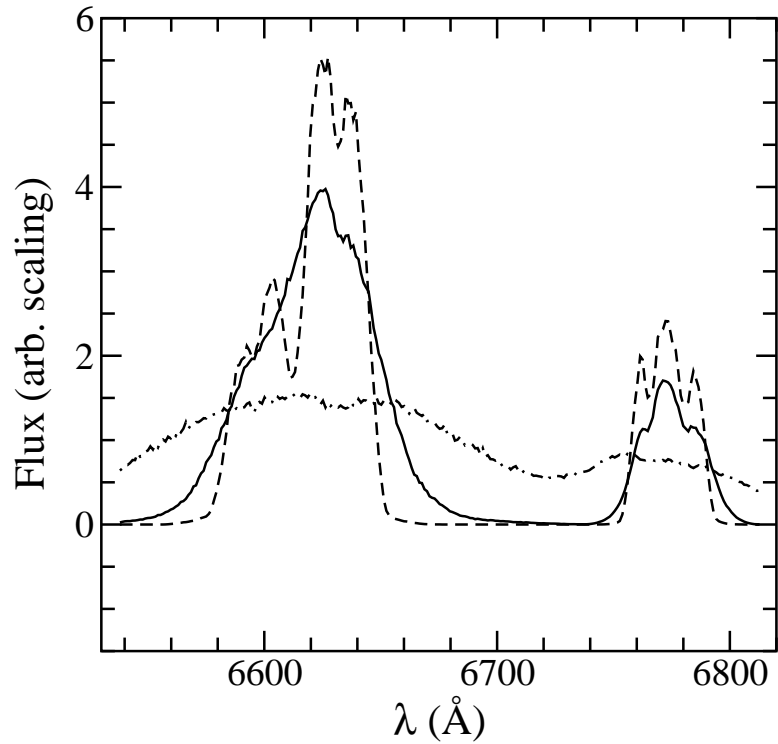


Fig. 6.— The dependence of the broad-line spectrum on the stress parameter α . Shown in the figure are the modeled spectra for $\alpha = 0.04$ (dot-dashed curve), $\alpha = 0.4$ (solid curve), and $\alpha = 1$ (dashed curve). The other parameters are fixed at: $L_{\text{ion}} = 4 \times 10^{40}$ erg/s, $n_o = 30000 \text{ cm}^{-3}$, $f = 0.045$, and $i = 64^\circ$.

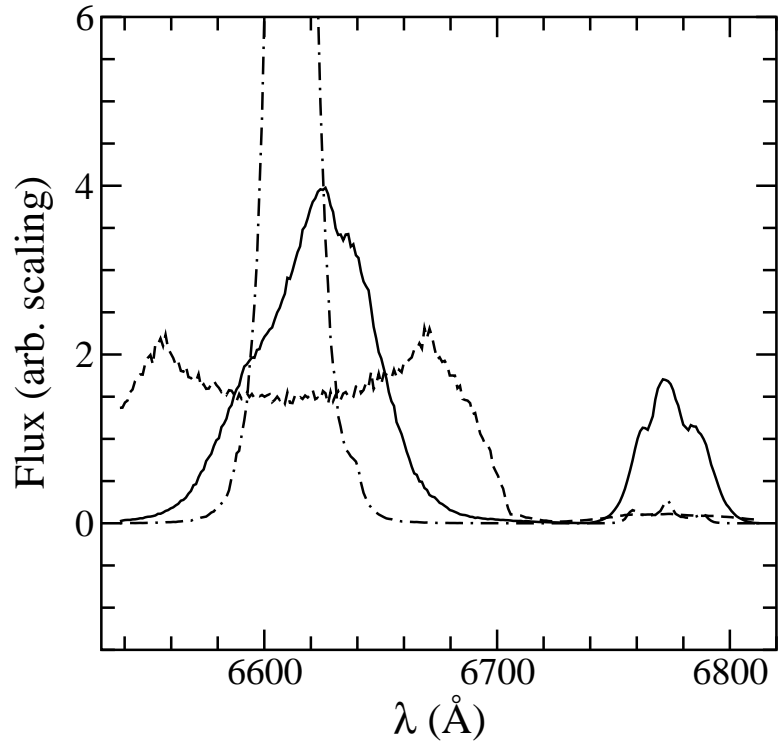


Fig. 7.— The dependence of the broad-line spectrum on the number density n_o of the disk at a distance of 10^{18} cm from the black hole. Shown in the figure are the modeled spectra for $n_o = 3000 \text{ cm}^{-3}$ (dot-dashed curve), $n_o = 30,000 \text{ cm}^{-3}$ (solid curve), and $n_o = 300,000 \text{ cm}^{-3}$ (dashed curve). The other parameters are fixed at: $L_{\text{ion}} = 4 \times 10^{40} \text{ erg/s}$, $\alpha = 0.4$, $f = 0.045$, and $i = 64^\circ$.

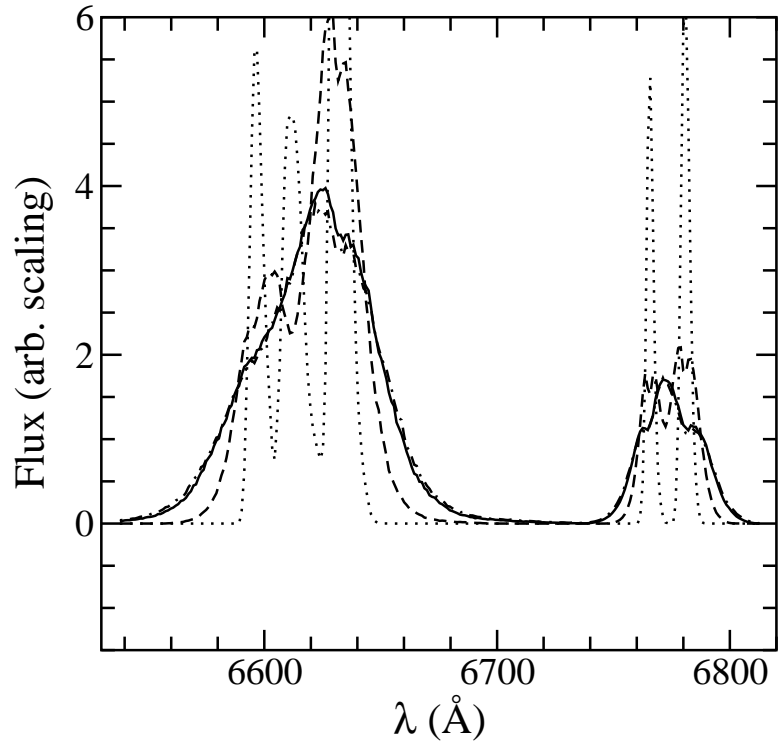


Fig. 8.— The dependence of the broad-line spectrum on the inclination angle of the disk i . Shown in the figure are the modeled spectra for $i = 0^\circ$ (dotted curve), $i = 30^\circ$ (dashed curve), $i = 64^\circ$ (solid curve), and $i = 75^\circ$ (dot-dashed curve). The other parameters are fixed at: $L_{\text{ion}} = 4 \times 10^{40}$ erg/s, $\alpha = 0.4$, $n_o = 30000$ cm $^{-3}$, and $f = 0.045$.

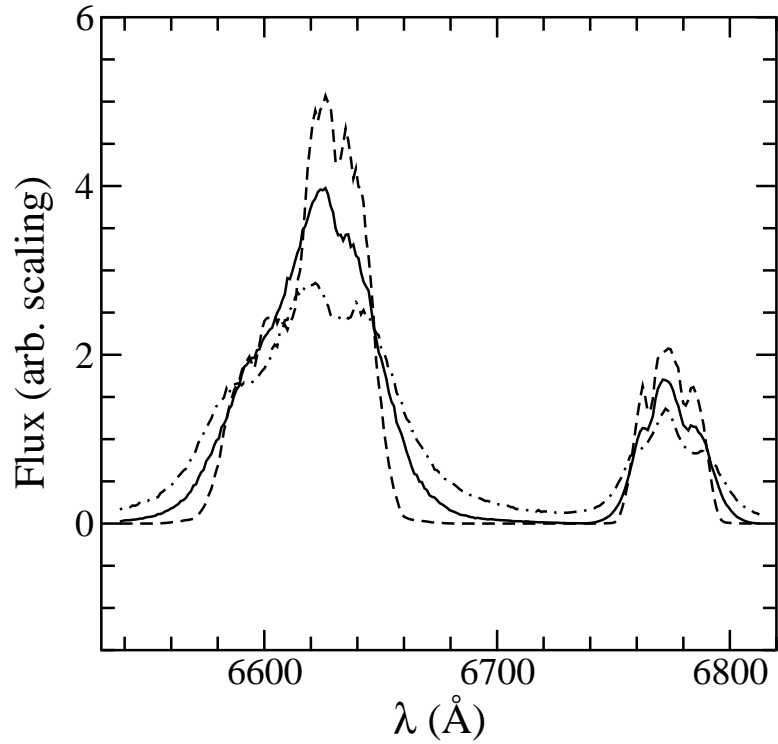


Fig. 9.— The dependence of the broad-line spectrum on the turbulence parameter f . Shown in the figure are the modeled spectra for $f = 0.011$ (dot-dashed curve), $f = 0.045$ (solid curve), and $f = 0.180$ (dashed curve). The other parameters are fixed at: $L_{\text{ion}} = 4 \times 10^{40}$ erg/s, $\alpha = 0.4$, $n_o = 30000 \text{ cm}^{-3}$, and $i = 64^\circ$.